Efficient Calibration of Cable-Driven Parallel Robots with Variable Structure

Dragoljub Surdilovic, Jelena Radojicic and Nick Bremer

Abstract This paper presents an efficient practical approach for the combined explicit and implicit approximated calibration of cable-driven parallel robots (wire robots, CDPR) mainly developed to tackle the problems with variable system structures, i.e. often reconfigurable common robot platform. Indeed, the developed calibration procedure can also be applied to the systems with stationary (end-effector-i.e. gripper-like) platforms, however the benefits of the new methods are mainly expressed in the variable structure systems. The variable structure CDPR systems cover classes of robots in which the common robot platform represents a working object to be manipulated, itself. Such systems are typical in novel CDPRs referred as *extended-cranes wire robots* or rehabilitation wire robots (e.g. STRINGMAN [1]). An additional specific system case belonging to the considered class is large mobile CDPR developed for applications in agriculture, which with changes of the application fields should be often periodically reconfigured and commissioned (calibrated). The paper provides detailed mathematical modelling of the novel calibration approach based on the parameter sensitivity analysis of the robot kinematic models including wire pulley systems. The implementation of the calibration procedures including required sensory systems and control supports has also been considered. Finally, practical examples illustrate the performance of the developed calibration method.

Keywords Wire-robots calibration · External- and self-calibration · Parameter sensitivity analysis · Sequential linear estimation · Force/impedance control · Wire tension

D. Surdilovic (✉) · J. Radojicic · N. Bremer
Department Robotics and Automation, Fraunhofer Institute for Production Systems and Design Technology IPK-Berlin, Pascalstr. 8-9, 10587 Berlin, Germany
e-mail: dragoljub.surdilovic@ipk.fraunhofer.de

A. Pott and T. Bruckmann (eds.), *Cable-Driven Parallel Robots*,
Mechanisms and Machine Science 32, DOI 10.1007/978-3-319-09489-2_9

1 Introduction

The *cable-driven parallel robots* (CDPR) or *wire-robots* have been recently addressed in numerous researches focusing on their advantages for implementing large spans, fast moving, lightweight and heavy-duty active spatial mechanisms. In comparison to a more general class of cable robots (e.g. spatial advanced robotized crane systems), the wire robots, especially the so called over-constrained structures, offer benefits such as ease of reconfiguration and adaptation to specific applications. Thereby the robot structures may be often changed, commonly by exchanging the working platform or varying locations of the robot wires attachments (pulleys, winches) in the space. Moreover, in specific CDPR systems, the change of common working platform or wire locations is closely related to the robot function.

A typical example represents the gait rehabilitation robot STRINGMAN [1]. This wire robot is unique, since its common platform interconnecting all cables represents the upper body of a patient (Fig. 1). The wires are connected to a harness carried by a patient performing gait training. The role of STRINGMAN is to provide weight suspension and gait balancing support (see [1] for more details). The procedures of patient attachments (Fig. 1) and detachments, facilitated by specific wire-tension control algorithms (based on force and impedance control) and patient lift-systems, represent a part of typical robot operations. The dimensions of the established "platform" practically vary for each patient, and efficient robot calibration and commissioning become crucial functions of the control system. Typical for the STRINGMAN are considerable inaccuracies, due to elasticity of the harness (human body attachment), which are tackled by the control system, relying on the interaction (force and impedance) control, rather than on the position control, supported by human tracking sensors (IMU, local wire-position sensors, vision etc.).

Another typical variable CDPR system requiring continuous calibration represents the so called *extended-crane systems* (Fig. 2). An extended-crane represents a combination of a wire robot and a conventional crane. The robot configuration is created to support task decomposition between the overhead crane (mainly performs

Fig. 1 STRINGMAN—patient attachments supported by lifting-system and wire-attach function (position based force/damping control)

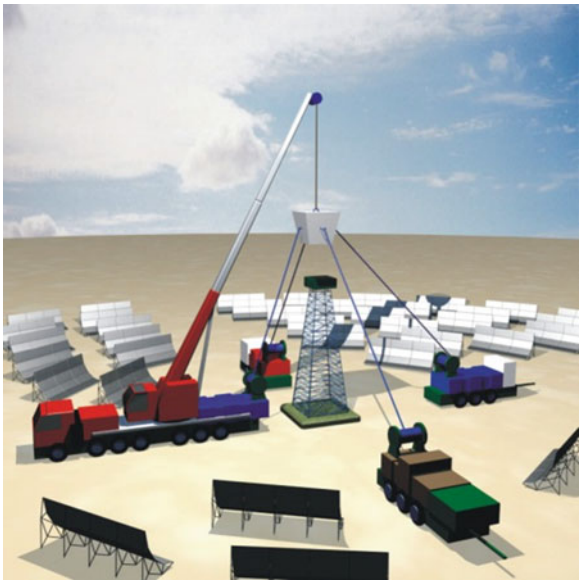

Fig. 2 Extended-crane system

the weight balancing and gross motion) and the side wire system (mainly responsible for fine lateral positioning and orientation). The extended crane can considerably improve flexibility and efficiency of assembly of heavy parts with complex irregular geometry. The side wires have been still applied for such operations in industrial practice but in pure manual manipulation form, to support fine-positioning of heavy parts carried by cranes. However, such repetitive operations are due to higher inertia of handling parts (ergonomic safe limit is ca. 20 kg) quite dangerous for human health and may cause serious back-pain problems. In extended crane systems the workpiece itself represents a common platform providing several attachment points. The side-wires (winches) carriers are commonly realized by mobile units with uncertain locations (Fig. 2). Fast calibration after commissioning, as well as following each new part attachment, should improve wire-robot models and model-based control.

A further example of variable structure and reconfigurable wire robot systems represent large CDPRs for agricultural applications (Fig. 3). To meet higher system flexibility and application requirements in various agricultural plants, it is convenient to implement these systems by means of mobile pillars that transport winches and platform, and can be fixed on stand-on legs at some locations to provide stable wire-robot structure [2]. The exact locations of winches thereby should be identified by calibration after system configuration/reconfiguration and commissioning.

Calibration, i.e. estimation of geometric and kinematic parameters of CDPRs, or in more general case of parallel robots, has been recently addressed in several researches [2–8]. Both system classes with characteristic structures, including closed-loops between attached legs/wires and platform, offer a specific possibility for the

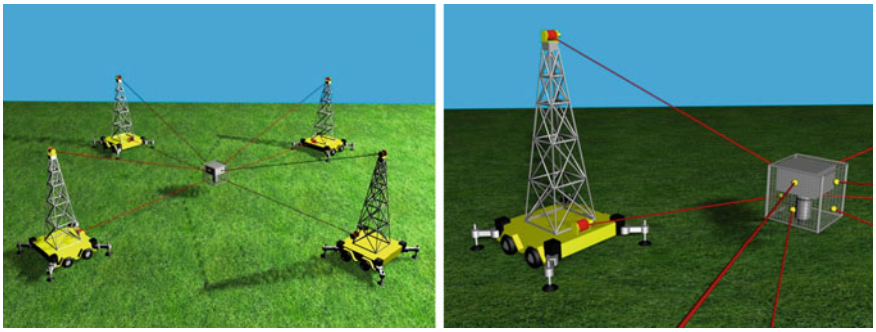

Fig. 3 Large wire-robots with mobile pillars for agricultural applications

calibration based only on internal (*proprioceptive*) sensing, referred to as "*implicit loop method*" [3]. As remarked by Wampler et all. [2], closed-loop relations provide additional information for calibrations that are equivalent to the end-point pose measurements in convenient industrial-robots with open kinematic chains. Additionally, redundancy of over-constrained wire-robots provides supplementary information for calibration [4]. The procedures for wire-robot calibration based on "implicit loop method" and proprioceptive sensors applications (e.g. local motor rotation/sliding sensors used for control purposes) are often referred to as *"self-calibration"* [4, 5]. Various specific self-calibration procedures (referred to as *tension-* and *jitter-based* self-calibration) have been developed in [6] for a planar wire-robot structures, in which some wires keep the length constant while remaining wires vary length or tension.

As is well known, the *self-calibration* in complex (e.g. non-negligible pulleys) and large wire-robots structures described by non-linear models, including wire cable elasticity [9, 10] with considerable parameter uncertainties may become also complex and converge to local minima that provide wrong information for identification. Linearized iterative methods that include direct-kinematics in the loop [6], also in general doesn't ensure convergence (contraction processes), producing the steps that deteriorate calibration procedure. Therefore complete identification schemes that tackle both parameter and pose uncertainties have been recently proposed [6].

In large scale robots (Figs. 2 and 3), however, the self-calibration procedure may become time-consumable and information from the external sensors can considerably improve the calibration, especially in non-linear systems with expressed cable sag and elasticity effects [8]. Thereby beside costly laser trackers [8] also relatively cheap sensors, such as cameras [3] or IMU's [1] (with additional external sensors, i.e. closed-loop based data fusion and drift compensation) may be applied.

This paper provides novel calibration methods that combine force/impedance control with external/internal CDPR calibration, which is based on affordable sensors and quite efficient for calibration of frequently reconfigurable wire-robots. This approach is based on an explicit linearized mathematical parameter sensitivity model of complex wires structures including pulleys. To cope with large dimension and

non-linearity, an approximation method based on sequential linear programming (SLP) and linear recursive approximations based on smaller calibration sub-problems [11] has been developed. Several simulation examples demonstrate the feasibility and robustness of the calibration performance against higher parametric deviations and measurement disturbances.

2 Kinematic Analysis

Kinematic models of wire-robots provides background for detailed parameter sensitivity analysis In Fig. 4, a general model of wire-robot with n-wires (i = 1,…, n) is given. In a over-constrained wire-robot structure ensuring 6DOF motion plus wires tension is $n \geq 7$. Using the notion from (Fig. 4), the position of the ith wire platform attachment point B_i is defined by

$$\mathbf{p}_i = \mathbf{a}_i + \mathbf{L}_i = \mathbf{p} + \mathbf{b}_i \tag{1}$$

where $\mathbf{a}_i$ and $\mathbf{b}_i$ are position vectors of pulley and platform attachment points A_i and B_i wrt. base and local platform frames respectively, $\mathbf{p}$ is the position vector of the platform reference frame and

$$\mathbf{L}_i = \overrightarrow{A_i C_i} + \overrightarrow{C_i T_i} + \mathbf{l}_i \tag{2}$$

where $\mathbf{l}_i$ is the wire-length vector, while C_i and T_i denote centre of the pulley and wire tangent points (Fig. 4).

During an arbitrary platform displacement, the wire performs a complex composite motion consisting of: *transferred motion*, representing the entire wire

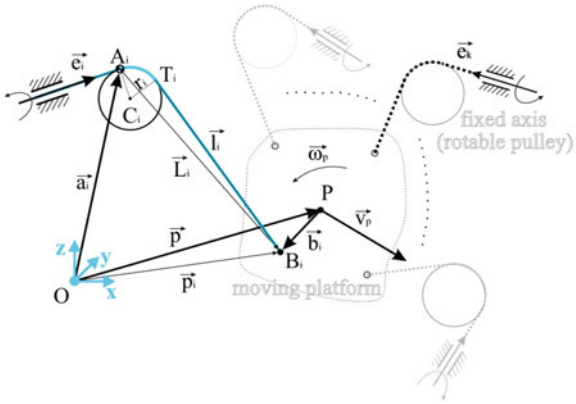

Fig. 4 Wire-robot structure

plane $\{A_i B_i C_i T_i\}$ rotation (rolling motion of the pulley) around the fixed pulley axis $\mathbf{e}_i$, and *relative motion* in the wire plane. The relative motion consists of relative translation i.e. change of the relative length in the actual cable direction (due to cable control, i.e. via a winch or linear slider mechanism (not presented in the Fig. 4), and a relative rotation of the wire around the pulley (i.e. point T_i that represents actual pole of the velocity). Based on this analysis, the expressions for absolute wire end-point velocities and accelerations are obtained

$$\mathbf{v}_i = \dot{\mathbf{p}}_i = \boldsymbol{\omega}_{ei} \times \mathbf{L}_i + \boldsymbol{\omega}_{ri} \times \mathbf{l}_i + \overset{*}{\mathbf{l}}_i = \mathbf{v}_p + \boldsymbol{\omega}_p \times \mathbf{b}_i \tag{3}$$

$$\mathbf{a}_i = \ddot{\mathbf{p}}_i = \boldsymbol{\varepsilon}_{ei} \times \mathbf{L}_i + \boldsymbol{\varepsilon}_{ri} \times \mathbf{l}_i + \boldsymbol{\omega}_{ei} \times (\boldsymbol{\omega}_{ei} \times \mathbf{L}_i) + \boldsymbol{\omega}_{ei} \times (\boldsymbol{\omega}_{ri} \times \mathbf{l}_i) + \boldsymbol{\omega}_{ri} \times (\boldsymbol{\omega}_{ri} \times \mathbf{l}_i) + 2(\boldsymbol{\omega}_e i + \boldsymbol{\omega}_{ri}) \times \overset{*}{\mathbf{l}}_i + \overset{**}{\mathbf{l}}_i = \mathbf{a}_p + \boldsymbol{\varepsilon}_p \times \mathbf{b}_i + \boldsymbol{\omega}_p \times (\boldsymbol{\omega}_p \times \mathbf{b}_i) \tag{4}$$

where $\boldsymbol{\omega}_{ei}$ and $\boldsymbol{\varepsilon}_{ei}$ denote pulley rotation velocity and acceleration around $\mathbf{e}_i$ (Fig. 5), $\boldsymbol{\omega}_{ri}$ and $\boldsymbol{\varepsilon}_{ri}$ relative wire rotation velocity and acceleration around wire-plane normal $\mathbf{n}_i$, $\overset{*}{\mathbf{l}}_i$ and $\overset{**}{\mathbf{l}}_i$ are linear wire relative velocity and acceleration due to cable length changes, $\mathbf{v}_p$ and $\boldsymbol{\omega}_p$, $\mathbf{a}_p$ and $\boldsymbol{\varepsilon}_p$ are platform linear and angular velocities and acceleration vectors respectively. Relative velocity components and their directions are shown in (Fig. 5). The projections of the velocity and acceleration vectors (3, 4) into wire-length vector direction, defined by unit vector $\mathbf{l}_{i0} = \mathbf{l}_i / l_i$, i.e. scalar multiplication of these equations by $\mathbf{l}_{i0}$ yields the magnitudes of wire linear relative velocity

$$\overset{*}{l}_i = [\mathbf{l}_{i0}{}^T \quad -\mathbf{l}_{i0}{}^T \underline{\underline{\mathbf{b}_i}}]\mathbf{t}_p \tag{5}$$

where $\mathbf{t}_p = [\mathbf{v}_p^T \quad \boldsymbol{\omega}_p^T]^T$ is the platform twist vector, while $\underline{\underline{\mathbf{b}_i}}$ denotes *skew-symmetric* 3×3 matrix formed from the elements of the vector $\mathbf{b}_i$ in order to represent the vector product in the matrix form. Scalar multiplication of (4) by $\mathbf{l}_{i0}$ yields the magnitude

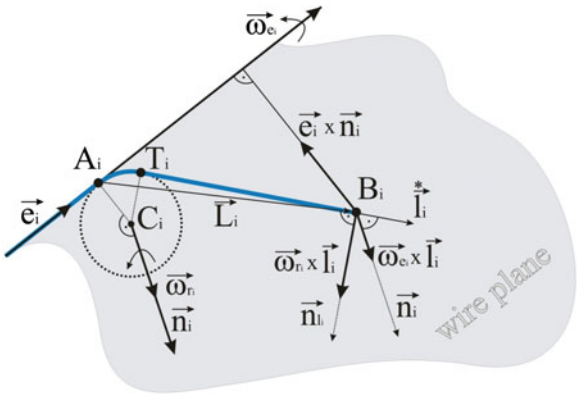

Fig. 5 Velocity vectors components

of wire relative acceleration

$$\overset{**}{l}_i = \omega_{e_i}^2[(\vec{\mathbf{e}}_i \times \vec{\mathbf{L}}_i)\cdot\vec{\mathbf{n}}_i][(\vec{\mathbf{e}}_i \times \vec{\mathbf{n}}_i)\cdot\vec{\mathbf{l}}_{i0}] + \omega_{r_i}^2 l_i + [\mathbf{l}_{i0}{}^T \quad -\mathbf{l}_{i0}{}^T \underline{\underline{\mathbf{b}_i}}]\dot{\mathbf{t}}_p - \mathbf{l}_{i0}{}^T \underline{\underline{\boldsymbol{\omega}_p}}\underline{\underline{\mathbf{b}_i}}\boldsymbol{\omega}_p \quad (6)$$

where the first two components represent the projections of centrifugal accelerations components (corresponding to the pulley and relative wire rotations), while the remaining parts define projections of platform tangential and centrifugal accelerations into the wire directions.

The expressions for vectors of angular pulley and wire relative rotations are obtained by scalar multiplication of (3) by vectors $\mathbf{n}_{l_i} = \mathbf{n}_i \times \mathbf{l}_{i0}$ and $\mathbf{n}_i$ respectively in terms of platform twist vector

$$\omega_{e_i} = \frac{1}{(\vec{\mathbf{e}}_i \times \vec{\mathbf{L}}_i)\cdot\vec{\mathbf{n}}_i}[\mathbf{n}_i^T - \mathbf{n}_i^T \underline{\underline{\mathbf{b}_i}}]\mathbf{t}_p \quad (7)$$

$$\omega_{r_i} = \frac{1}{l_i}[-\mathbf{l}_{i0}{}^T \underline{\underline{\mathbf{n}_i}} \quad \mathbf{l}_{i0}{}^T \underline{\underline{\mathbf{n}_i}}\underline{\underline{\mathbf{b}_i}}]\mathbf{t}_p \quad (8)$$

3 Wire-Robot Jacobian and Its Time-derivative

The relationship between relative wire velocity, defining the cable length variations, and platform twist vector is defined by the wire-robot Jacobian

$$\overset{*}{\mathbf{l}} = \mathbf{J}\mathbf{t}_p \quad (9)$$

where $\overset{*}{\mathbf{l}} = [\overset{*}{l}_1 \ldots \overset{*}{l}_i \ldots \overset{*}{l}_n]^T$ and Jacobian matrix $\mathbf{J} \in \Re^{n\times 6}$ is

$$\mathbf{J}^T = \begin{bmatrix} \mathbf{l}_{10} & \cdots & \mathbf{l}_{i0} & \cdots & \mathbf{l}_{n0} \\ \underline{\underline{\mathbf{b}_1}}\mathbf{l}_{10} & \cdots & \underline{\underline{\mathbf{b}_i}}\mathbf{l}_{i0} & \cdots & \underline{\underline{\mathbf{b}_n}}\mathbf{l}_{n0} \end{bmatrix} \quad (10)$$

The time derivative of wire Jacobian is obtained by differentiating (9) (the same result is obtained by substituting (7) and (8) in (6))

$$\overset{**}{\mathbf{l}} = \mathbf{J}\dot{\mathbf{t}}_p + \dot{\mathbf{J}}t_p \quad (11)$$

where based on (10) is

$$\dot{\mathbf{J}}^T = \begin{bmatrix} \dot{\mathbf{l}}_{10} & \cdots & \dot{\mathbf{l}}_{i0} & \cdots & \dot{\mathbf{l}}_{n0} \\ \underline{\dot{\mathbf{b}}_1}\mathbf{l}_{10} + \underline{\mathbf{b}_1}\dot{\mathbf{l}}_{10} & \cdots & \underline{\dot{\mathbf{b}}_i}\mathbf{l}_{i0} + \underline{\mathbf{b}_i}\dot{\mathbf{l}}_{i0} & \cdots & \underline{\dot{\mathbf{b}}_n}\mathbf{l}_{n0} + \underline{\mathbf{b}_n}\dot{\mathbf{l}}_{n0} \end{bmatrix} \quad (12)$$

Taking into account that the time derivatives of the constant intensity vectors $\mathbf{l}_{i0}$ and $\mathbf{b}_i$ (considering an ideal rigid platform) are

$$\begin{aligned} \dot{\mathbf{l}}_{i0} &= \boldsymbol{\omega}_{e_i} \times \mathbf{l}_{i0} + \boldsymbol{\omega}_{r_i} \times \mathbf{l}_{i0} \\ \dot{\mathbf{b}}_i &= \boldsymbol{\omega}_i \times \mathbf{b}_i \end{aligned} \tag{13}$$

and substituting (7) and (8) yields

$$\dot{\mathbf{J}} = \mathbf{t}_p^T \otimes \mathbf{J} = \mathbf{t}_p^T \otimes [\mathbf{J}_1^T \dots \mathbf{J}_{\mathrm{i}}^T \dots \mathbf{J}_{\mathrm{n}}^T]^T \tag{14}$$

where $\mathbf{J}$ is a $n(6) \times 1(6)$ block matrix (numbers outside parenthesis define block matrix dimension, while within parenthesis the dimension of each block-matrix element has been given), $\otimes$ is the Kronecker's product (each block-element of $\mathbf{J}$ is by $\mathbf{t}_p^T$ multiplied) and the block element $\mathbf{J}_{\mathrm{i}} \in \Re^{6\times 6}$ has the form

$$\mathbf{J}_{\mathrm{i}} = \begin{bmatrix} -\frac{1}{l_i}\underline{\underline{\mathbf{n}_i}}\underline{\underline{\mathbf{l}_{i0}}}\underline{\underline{\mathbf{l}_{i0}}}^T\underline{\underline{\mathbf{n}_i}} - \frac{1}{(\vec{\mathbf{e}}_i \times \vec{\mathbf{L}}_i)\cdot\vec{\mathbf{n}}_i}\mathbf{n}_i\mathbf{l}_{i0}{}^T\underline{\underline{\mathbf{e}_i}} & \frac{1}{l_i}\underline{\underline{\mathbf{n}_i}}\underline{\underline{\mathbf{l}_{i0}}}\underline{\underline{\mathbf{l}_{i0}}}^T\underline{\underline{\mathbf{n}_i}}\underline{\underline{\mathbf{b}_i}} + \frac{1}{(\vec{\mathbf{e}}_i \times \vec{\mathbf{L}}_i)\cdot\vec{\mathbf{n}}_i}\mathbf{n}_i\mathbf{l}_{i0}{}^T\underline{\underline{\mathbf{e}_i}}\underline{\underline{\mathbf{b}_i}} \\ -\frac{1}{l_i}\underline{\underline{\mathbf{b}_i}}\underline{\underline{\mathbf{n}_i}}\underline{\underline{\mathbf{l}_{i0}}}\underline{\underline{\mathbf{l}_{i0}}}^T\underline{\underline{\mathbf{n}_i}} - \frac{1}{(\vec{\mathbf{e}}_i \times \vec{\mathbf{L}}_i)\cdot\vec{\mathbf{n}}_i}\underline{\underline{\mathbf{b}_i}}\mathbf{n}_i\mathbf{l}_{i0}{}^T\underline{\underline{\mathbf{e}_i}} & \frac{1}{l_i}\underline{\underline{\mathbf{b}_i}}\underline{\underline{\mathbf{n}_i}}\underline{\underline{\mathbf{l}_{i0}}}\underline{\underline{\mathbf{l}_{i0}}}^T\underline{\underline{\mathbf{n}_i}}\underline{\underline{\mathbf{b}_i}} + \frac{1}{(\vec{\mathbf{e}}_i \times \vec{\mathbf{L}}_i)\cdot\vec{\mathbf{n}}_i}\underline{\underline{\mathbf{b}_i}}\mathbf{n}_i\mathbf{l}_{i0}{}^T\underline{\underline{\mathbf{e}_i}}\underline{\underline{\mathbf{b}_i}} + \underline{\underline{\mathbf{b}_i}}\underline{\underline{\mathbf{l}_{i0}}} \end{bmatrix} \tag{15}$$

4 Parameter Sensitivity Model

The kinematic model sensitivity analysis provides a framework for the development of the calibration procedure. The above presented CDPR kinematic model includes several parameters definitions: robot structure (vectors $\vec{\mathbf{e}}_i$ and $\vec{\mathbf{a}}_i$, pulley radius r_i), platform dimension, i.e. wire attachment points (vectors $\tilde{\mathbf{b}}_i$, where $\tilde{\cdot}$-denotes vectors in local-platform coordinate systems), and variable platform position and rotation vectors $\mathbf{x}_p = [\mathbf{p}_p^T \quad \mathbf{o}_p^T]^T$. The rotation vector $\mathbf{o}_p$ takes different forms dependent on selected rotation presentation (e.g. axis-angle, Cardan-, Euler- etc. angles). The measurable wire length s_i, on a sliding- or a winch drive, consists of the active wire-length l_i and the pulley arc of the contact length (Fig. 6). The basic kinematic relationships for the calibration thus include

$$\begin{aligned} s_i &= r_i\delta_i + l_i \\ \mathbf{p}_i &= \mathbf{a}_i + \mathbf{L}_i = \mathbf{p} + \mathbf{b}_i = \mathbf{p} + \mathbf{R}\tilde{\mathbf{b}}_i \\ \mathbf{L}_i &= \overrightarrow{A_iC_i} + \overrightarrow{C_iT_i} = r_i\left[\vec{e}_i \times \vec{n}_i - \frac{1}{l_i}l_i \times \vec{n}_i\right] \end{aligned} \tag{16}$$

where $\delta_i \ =\prec \ A_iT_i$ is the circular segment angle between points A_i and T_i (see Fig. 6). The kinematic *loop closure* between two wire chains i and j over the platform requires additionally

$$\mathbf{a}_i - \mathbf{a}_j + \mathbf{L}_i - \mathbf{L}_j = \mathbf{R}(\tilde{\mathbf{b}}_i - \tilde{\mathbf{b}}_j) \tag{17}$$

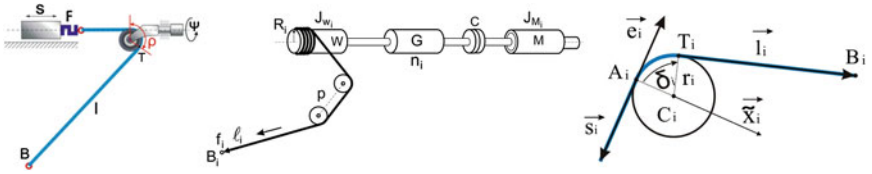

Fig. 6 Wire transmission chains with linear sliders (*left*) and winches (*right*)

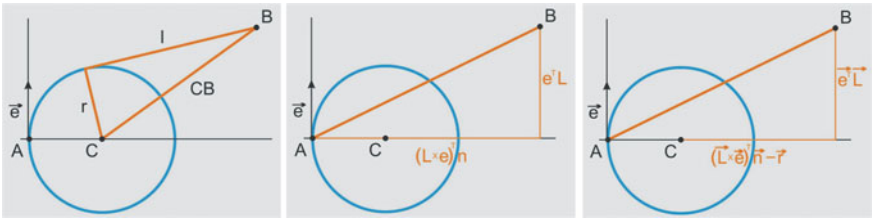

Fig. 7 Right-triangles relationships

The kinematic model parameters (16–17) uniquely define the position and orientation of platform, i.e. wire attachment points B_i, in the space. By means of these parameters two basic kinematic tasks *inverse* (*IK*) and *direct-forward kinematics* (*DK*) can be solved. The *IK* is trivial in CDPRs, mainly based on simple geometric considerations: starting from given $\mathbf{x}_p$, i.e. known B_i, determining the tangent on pulley (Thales' circle), following by computation of δ_i and finally s_i (16). Further transformation to corresponding motor angle or linear drive position is also easy and depends on specific transmission train (Fig. 7). As well known, *DK* that determines platform pose starting from measured s_i appears to be more complex in parallel manipulators, and has been usually solved by iterative numeric procedures [9] optimized for real-time applications (control).

In the reconfigurable systems, however, the fixed wire-robot parameters ($\vec{\mathbf{e}}_i, \vec{\mathbf{a}}_i, \tilde{\vec{\mathbf{b}}}_i$) are unknown or uncertain and should be estimated before operation. The linearization of (16) around an initial nominal parameter-model configuration ($\vec{\mathbf{e}}_{i0}, \vec{\mathbf{a}}_{i0}, \tilde{\vec{\mathbf{b}}}_{i0}$) and an initial model pose ($\mathbf{p}_0, \mathbf{R}_0$) yields

$$\begin{aligned} \Delta\mathbf{a}_i + \Delta\mathbf{L}_i &= \Delta\mathbf{p} + \mathbf{R}_0\, \Delta\tilde{\mathbf{b}}_i + \underline{\underline{\Delta\mathbf{o}}}\, \mathbf{R}_0\tilde{\mathbf{b}}_{i0} \\ \Delta s_i &= r_i\, \Delta\delta_i + \Delta l_i \end{aligned} \tag{18}$$

where $\underline{\underline{\Delta\mathbf{o}}}$ represents skew-symmetric matrix of infinitesimal platform rotations. The above equations provide a framework for a complete identification concerning both parameter and pose uncertainties.

The efficiency of the calibration can be improved by considering explicit dependency between wire-robot parameters ($\vec{\mathbf{e}}_i$, $\vec{\mathbf{a}}_i$, $\vec{\tilde{\mathbf{b}}}_i$) and cable length Δl_i (Δs_i) deviations

$$l_i = l_i\left(\mathbf{a}_i, \tilde{\mathbf{b}}_i, \mathbf{e}_i, \mathbf{p}, \mathbf{o}\right) = l_i\left(\mathbf{a}_i, \tilde{\mathbf{b}}_i, \mathbf{e}_i, \mathbf{x}\right) \tag{19}$$

and

$$\begin{aligned} dl_i &= \frac{\partial l_i}{\partial \mathbf{x}^T} d\mathbf{x} + \frac{\partial l_i}{\partial \tilde{\mathbf{b}}_i^T} d\tilde{\mathbf{b}}_i + \frac{\partial l_i}{\partial \mathbf{a}_i^T} d\mathbf{a}_i + \frac{\partial l_i}{\partial \mathbf{e}_i^T} d\mathbf{e}_i \\ \Delta l_i &= \frac{\partial l_i}{\partial \mathbf{x}^T} \Delta\mathbf{x} + \frac{\partial l_i}{\partial \tilde{\mathbf{b}}_i^T} \Delta\tilde{\mathbf{b}}_i + \frac{\partial l_i}{\partial \mathbf{a}_i^T} \Delta\mathbf{a}_i + \frac{\partial l_i}{\partial \mathbf{e}_i^T} \Delta\mathbf{e}_i \end{aligned} \tag{20}$$

The relationship between Δl_i and the platform pose deviations $\Delta\mathbf{x} = \left[\, \Delta\mathbf{p}^T \;\; \Delta\mathbf{o}^T \,\right]^T$ is governed by the wire-robot Jacobian (9–10).

$$\frac{\partial l_i}{\partial \mathbf{x}^T} = \left[\, {\mathbf{l}_{i0}}^T \;\; -{\mathbf{l}_{i0}}^T \underline{\underline{\mathbf{b}}}_i \,\right] \tag{21}$$

The Jacobian (10) and the equivalence between linear displacement $\Delta\mathbf{p}$, i.e. $\Delta\mathbf{p}_i$, and platform parameters deviations $\Delta\tilde{\mathbf{b}}_i$, given by $\Delta\mathbf{p}_i = \mathbf{R}\Delta\tilde{\mathbf{b}}_i$, yields

$$\frac{\partial l_i}{\partial \tilde{\mathbf{b}}_i^T} = {\mathbf{l}_{i0}}^T \tag{22}$$

The partial derivatives of l_i with respect to remaining parameter vectors may be computed based on the geometrical relations in right triangles (Fig. 7)

$$\begin{aligned} l_i^2 &= \overline{C_i B_i}^2 - r_i^2 \\ \overline{C_i B_i}^2 &= (\mathbf{L}_i \cdot \mathbf{e}_i)^2 + ((\mathbf{L}_i \times \mathbf{e}_i) \cdot \mathbf{n}_i - r_i)^2 \\ L_i^2 &= (\mathbf{L}_i \cdot \mathbf{e}_i)^2 + ((\mathbf{L}_i \times \mathbf{e}_i) \cdot \mathbf{n}_i)^2 \end{aligned} \tag{23}$$

yielding

$$l_i^2 = L_i^2 - 2\left((\mathbf{L}_i \times \mathbf{e}_i) \cdot \mathbf{n}_i\right)^2 \tag{24}$$

From (23–24), considering generalized partial derivative transformation

$$\frac{\partial l_i}{\partial \mathbf{u}_i^T} = \frac{\partial \left(l_i^2\right)^{1/2}}{\partial \mathbf{u}_i^T} = \frac{1}{2l_i} \frac{\partial \left(l_i^2\right)}{\partial \mathbf{u}_i^T} = \frac{1}{2l_i} \frac{\partial \left(L_i^2 - 2r_i\left(\mathbf{L}_i \times \mathbf{e}_i\right) \cdot \mathbf{n}_i\right)}{\partial \mathbf{u}_i^T} \tag{25}$$

and taking into account the relationships

$$\frac{\partial L_i^2}{\partial \mathbf{a}_i^T} = -2\mathbf{L}_i^T \text{ and } \frac{\partial\left((\mathbf{L}_i \times \mathbf{e}_i)\cdot \mathbf{n}_i\right)}{\partial \mathbf{a}_i^T} = -\left(\mathbf{e}_i \times \mathbf{n}_i\right)^T \tag{26}$$

yields the desired partial derivatives with respect to $\mathbf{a}_i$

$$\frac{\partial l_i}{\partial \mathbf{a}_i^T} = \frac{1}{l_i}\left(-\mathbf{L}_i^T + r_i(\mathbf{e}_i \times \mathbf{n}_i)^T\right) = -\frac{1}{l_i}\overrightarrow{C_i B_i}^T \tag{27}$$

In other words, an infinitesimal variation $\delta\,\mathbf{a}_i$ that is orthogonal to $\overrightarrow{C_i B_i}$ doesn't cause the variation of the cable length $\delta l_i = 0$ (Fig. 8).

Finally the variations δe_i which are compatible with other constraints (small rotations of e_i around A_i), cause

$$\frac{\partial l_i}{\partial \mathbf{e}_i^T} = \frac{r_i}{l_i}\frac{\mathbf{L}_i^T\mathbf{e}_i}{(\mathbf{L}_i \times \mathbf{e}_i)\cdot \mathbf{n}_i}\mathbf{L}_i^T \tag{28}$$

Due to constrained space the proof of (28), which is also based on relationship (23–25), as well as on the statement that $\mathbf{L}_i$ is not changed during e_i variations (points A_i and B_i remain fixed) (Fig. 5), is omitted. The deviations δe_i of pulley axes are related to small angular rotations (errors) around two orthogonal axes defined by the rotation vector $\delta\, o_i$ with respect to a local coordinate frame attached to the e_i. This relationship is defined by

$$\delta e_i = \delta o_i \times e_i = \underline{\underline{\delta o_i}}\, e_i = -\underline{\underline{e_i}}\,\delta o_i = -R_i \underline{\underline{\tilde{e}_i}}\, R_i^T \delta o_i = -R_i \underline{\underline{\tilde{e}_i}}\,\delta\tilde{o}_i \tag{29}$$

where "$\sim$" denotes vectors defined by projections into local frames, R_i is rotation matrix of this frame with respect to the base coordinate system. Substituting (29) into (28) defines parameter sensitivity of the l_i variations to small axis e_i deviations $\delta\tilde{\mathbf{o}}_i = [\,\delta\tilde{o}_{ix}\ \delta\tilde{o}_{iy}\ 0\,]$.

The parameter sensitivity model (17–29) provides a framework for the development of novel calibration procedures that is described in the following.

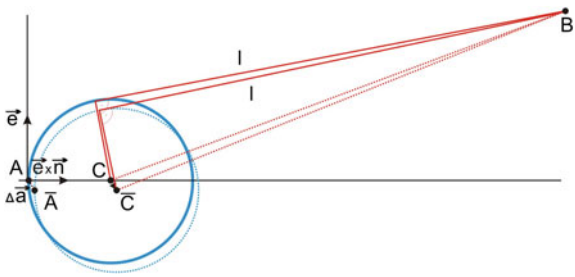

Fig. 8 Geometric proof of (26)—virtual displacement in direction orthogonal to $\vec{C_i B_i}$ doesn't produce wire-length changes (δl_i=0)

5 Calibration Procedure

Let us consider the extended-crane system in (Fig. 9) and the large over-constrained agricultural robots (Fig. 10). In principle, the calibration starts from a new wire-robot (on the example of an extended-crane) to be configured by attaching the wires to the common-workpiece (platform). At the beginning the winches have been fixed at known but uncertain locations defined by $\boldsymbol{a}_i$ w.r.t. a base frame of reference. The crane transports the workpiece to the assembly locations and the operator can manually attach the wires using local winch force/impedance (precisely damping) control. Thereby the wire-tension, i.e. force sensors, built in all winches (see [13] for more details), including also the main crane wire, have been utilized. After attachment, the tension wire control ensures the tension of all wires that are required to fix the workpiece in a desired, but also uncertain pose $\mathbf{x}_j(\mathrm{j} = 1 \ldots \mathrm{N}_x)$, where N_x denotes number of poses used in calibration. The local wires have been calibrated to provide an effective wire length measurements $s_i(\mathrm{i} = 1, \ldots \mathrm{n})$ of the winches, for each pose. For the measurements of $\mathbf{x}_j$ after initial point calibration (details have been also omitted), various sensors such as IMU's with additional drift compensation sensors (including also internal implicit wire-robot sensors and constraints equations) and Kalman-filtering techniques may be used (it is not the focus of this paper).

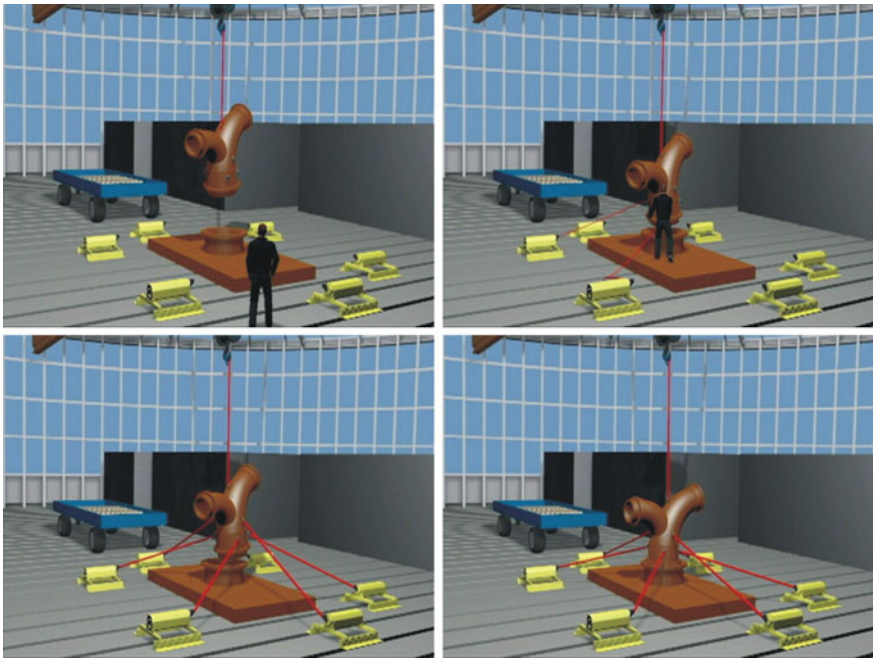

Fig. 9 Configuration of an extended crane system: transportation, wires attachment and tension

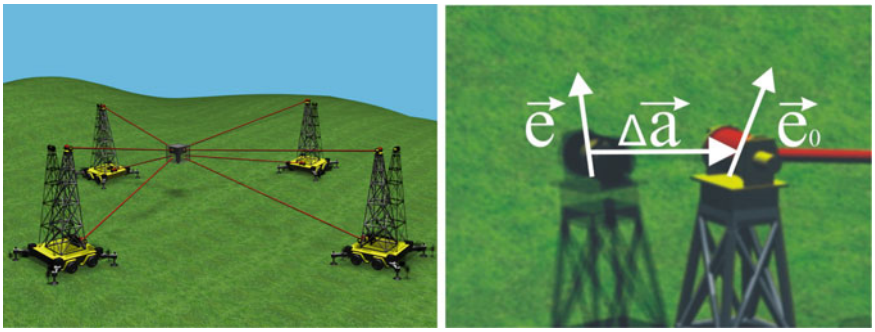

Fig. 10 Deviation model of a large span wire-robot

During calibration the platform moves to the poses $\mathbf{x}_j$, for example by combining the Cartesian space jogging and wire-tension control ensuring a steady-state stable pose. A previous selection of the points (calibration experiment design ensuring some optimality criterion, see [14]), may considerably improve the quality of identification, however, it is also out of the scope of this paper.

Calibration can be described briefly as the following problem. For the given set of measurements $M = \{\mathbf{x}_j, s_i(\mathbf{x}_j)\}$, and initial (model) parameters values $\hat{P} = \{\hat{\mathbf{a}}_i, \hat{\tilde{\mathbf{b}}}_i, \hat{\mathbf{e}}_i\}$, identify the system parameters $P = \{\mathbf{a}_i, \tilde{\mathbf{b}}_i, \mathbf{e}_i\}$ that in an optimal way fit the set of measurements and kinematic model constraints (17–21).

The calibration procedure involves the following linear approximation steps (***Algorithm 1***):

- Estimation of initial wire lengths based on the IK model

$$\hat{l}_{ij} = l_i^{-1}\left(\hat{\mathbf{a}}_i, \hat{\tilde{\mathbf{b}}}_i, \hat{\mathbf{e}}_i, \mathbf{x}_j\right)$$

- Estimation of wire active lengths based on total cable length measurements taking nominal values for the non-measurable wire contact arc $\delta_{ij} \approx \hat{\delta}_{ij}$ based on

$$\bar{l}_{ij} = s_{ij} - r_i \delta_{ij}$$

- Optimal fitting of parameters by minimizing cable length errors (squares) $\Delta l_{ij} = \bar{l}_{ij} - \hat{l}_{ij}$. Using derived explicit sensitivity model (26) this leads to solving a linear regression problem, in the considered case

$$\Delta \mathbf{a} = inv\left(\mathbf{R}^T\mathbf{R}\right)\mathbf{R}^T\Delta \mathbf{l}_{N_j}$$

where the regression matrix $\mathbf{R} \in \Re^{N_j \cdot n \times n \cdot 3}$ includes parameter Jacobians (10).

In the illustrative example, 20 platform measuring points have been selected nearly to the middle of the working space (which may be realized by practical tensions)

(Fig. 10). Instead of an extended crane, an over-constrained robot with n=8 wires has been considered. This robot represents an example of large agricultural wire-robot (Fig. 10) with the nominal span of 100 m and relatively large parameter perturbations. For the sake of simplicity only estimation of **a** will be considered. For this purpose a set of the following attachment points for simulating measurements has been selected

$$\mathbf{a}_0 = \begin{bmatrix} 50 & -50 & -50 & 50 & 50 & -50 & -50 & 50 \\ 50 & 50 & -50 & -50 & 50 & 50 & -50 & -50 \\ 25 & 25 & 25 & 25 & 0 & 0 & 0 & 0 \end{bmatrix}$$

As initial model parameters the following vector has been selected with a relatively large initial deviation 2-norm of $\Delta \mathrm{a}(0) \approx 4$ (m)

$$\hat{\mathbf{a}} = \begin{bmatrix} 46.9980 & -52.3952 & -51.0638 & 51.9303 & 48.0770 & -51.5475 & -50.4222 \\ 48.1406 & 52.0706 & 47.5845 & -53.0748 & -50.4700 & 52.5282 & 53.4440 \\ -50.2576 & -48.4173 & 22.3897 & 28.2407 & 26.6444 & 22.3588 & -2.8097 \\ & & & & -3.4949 & 1.3985 & 2.3109 \end{bmatrix}$$

If we neglect the position measurements errors (ideal sensors case), the Algorithm 1 converges very fast, reducing the initial errors after only few steps to 2-norm $\Delta \mathrm{a} \approx 10^{-10}$(m). The cable length (and contact arc angles δ_{ij}) residuum become also almost nullified.

However, this is a very simplified case that doesn't meet the practice, since the platform position measurements are also erroneous. Therefore the position errors have been randomly added to any measurements with again relative large errors, with uniform distribution errors and 2-norm $\Delta x(0) \approx 0.04$ (m). When the errors have been included, the linear regression fitting converges to an optimum with relatively large deviations and 2-norm $\Delta \mathrm{a}(4) \approx 0.1987$ (m). Thereby relatively large residuum's of cable lengths 2-norm $\Delta \mathrm{l}(4) \approx 0.0415$(m) (often of the same order as initial $\Delta \mathbf{x}$) has been achieved, where the index in parenthesis denotes number of iterations.

These residua cannot be reduced by further iterations since a local optimum has been reached. In order to advance the calibration, a logical improvement may be the estimation of both $\Delta \mathbf{a}$ and position errors measurements $\Delta \mathbf{x}$. However, this leads to a large linear optimization problem with commonly very bad conditioning and scaling of the regressor. The linear constrained fitting algorithms may limit parameters exploding, however, bad convergence and numerical errors remains typical problems. In order to tackle these limitations, a next *sequential optimization* step has been proposed.

The aim of the next sequential sub-estimation step (***Algorithm 2***) is to

- identify position errors by means of the wire robot Jacobian and thus to reduce (commonly after next few steps 2-norm $\Delta \mathrm{l} < 0.0001$(m);
- reduce further the residuum $\Delta \mathrm{a}$ by performing sequential optimization with more stable fitting of smaller problems. Thereby both $\Delta \mathbf{x}$ and $\Delta \mathbf{a}$ gradients have to be computed iteratively.

As a result the cable length error can be considerably improved, while $\Delta\mathbf{a}$ reduction remains usually not significant (0.10 m) (dependent on selected start points).

To remove further $\Delta\mathbf{a}$ errors, finally the following sub-problem has to be solved (***Algorithm 3***)

- *self-calibration* by checking all possible closed loops with the wires based on (17–19) (there are totally 28 loop closure equations for each point in the considered case).

After this step finally the typical results have been achieved: 2-norm $\Delta\mathbf{a} < 0.01$ (m), while 2-norm $\Delta\mathbf{l} < 10^{-4}$(m) has been kept small by iterative position errors estimations.

Commonly all the above *Algorithms* steps require a few iterations (4–6) representing smaller sub-problems and are quite suitable for real-time applications.

$$\begin{aligned}\mathbf{a} = [&50.0032 \; -49.9968 \; -49.9968 \; 50.0032 \; 50.0032 \; -49.9968 \; -49.9968\\ &50.0032 \; 49.9905 \; 49.9905 \; -50.0095 \; -50.0095 \; 49.9905 \; 49.9905\\ &-50.0095 \; -50.0095 \; 25.0025 \; 25.0025 \; 25.0025 \; 25.0025 \; 0.0025\\ &0.0025 \; 0.0025 \; 0.0025]\end{aligned}$$

It is worth mentioning that the calibration of pulley axes orientation errors $\delta\tilde{\mathbf{o}}_i$ appears to be sensitive to the wire contact arc $\delta_{ij} \approx \hat{\delta}_{ij}$ errors which are not measurable. Therefore the calibration of these angles based on both parameter sensitivity model and internal loop closure must be performed synchronously.

6 Conclusion

This paper has presented the detailed modeling of wire-robot kinematic models parameter sensitivity and application for calibration in general wire-robot systems with pulley elements. The novel algorithms include exact mathematical models to avoid complex numerical procedures and apply sequential gradient methodology to cope with large parameters fitting and bad conditioning problems.

The developed calibration procedures appear to be especially effective for variable structure CDPR systems, which cover classes of robots in which the common robot platform represents a working object to be manipulated, itself. Such systems are typical in novel CDPRs referred as *extended-cranes wire robots* under development at IPK. An illustrative example presents the performance of the developed calibration algorithms for large-scale cable robots with relatively higher parameter uncertainities.

The future work will focus on implementation in the mock-up extended crane system of which a presentation has been planned in September 2014.

Acknowledgments The work presented in this paper has been partially funded by Fraunhofer Community within WISA-ATLAS Project focusing on automated assembly of large-scale structures by means of wire robotic systems.

References

1. Surdilovic D, Bernhardt R, Schmidt T, Zhang J (2004) STRING-MAN: a novel wire robot for gait rehabilitation. In: Advances in rehabilitation robotics, Lecture Notes in Control and Information Science, Springer-Verlag, vol 306, 2004, pp 413–424
2. Wampler CW, Hollerbach JM, Arai T (1995) An implicit loop method for kinematic calibration and its application to closed-chain mechanisms. IEEE Trans Robot Autom 11(5):710–724
3. Traslosheros A, Sebastian JM, Torrijos J, Carelli R, Castillo E (2013) An inexpensive method for kinematic calibration of a parallel robot by using one hand-held camera as main sensor. Sensors 13:9941–9965
4. Miermeister P, Pott A, Verl A (2012) Auto-calibration method for overconstrained cable-driven parallel robots. In: 7th German conference on robotics (ROBOTIK 2012), Proceedings CD-ROM, Berlin VDE-Verlag, 2012, pp 301–306
5. Borgstrom PH, Jordan BL, Borgstrom BJ, Sukhatme GS, Batalin MA, Kaiser WJ (2009) NIMS-PL: a cable-driven robot with self-calibration capabilities. IEEE Trans Robot 25(5):1005–1015
6. Dit Sandretto JA, Daney D, Gouttefarde M, Baradat C (2012) Calibration of a fully-constrained parallel cable-driven robot. In: 19th CISM-IFToMM symposium on robot design, dynamics and Control (ROMANSY 2012), Paris
7. Miermeister P, Pott A (2013) Auto-calibration method for cable-driven parallel robots using force sensors. In: Latest Advances in Robot Kinematics, 1st international conference on cable-driven parallel robots, Stuttgart, 2012, Springer (2013)—Mechanisms and Machine Science, pp 269–276
8. Duan X, Qiu Y, Duan Q, Du J (2014) Calibration and motion control of a cable-driven parallel manipulator based triple-level spatial positioner, Hindawi Publishing Corporation, Advances in Mechanical Engineering, vol 2014, Article ID 368018, p 10
9. Merlet JP (2008) Analysis of wire elasticity for wire-driven parallel robots. In: Proceedings of EuCoMeS, 2nd European conference on mechanism science, Cassino (Italy), 2008
10. Surdilovic D, Radojicic J, Krüger J (2013) Geometric stiffness analysis of wire robots: a mechanical approach. In: 1st international conference on cable-driven parallel robots, Stuttgart, 2012, Springer (2013)—Mechanisms and Machine Science, pp 389–404
11. Radojicic J, Surdilovic D, Krüger J (2013) Application challenges of large-scale wire robots in agricultural plants. In: Proceedings of 2013 IFAC bio-robotics conference, vol 1, Part 1, pp 77–82
12. Lamberti L, Pappalettere C (2002) Design optimization of large-scale structures with sequential linear programming. Proc Inst Mech Eng C: J Mech Eng Sci 216:799
13. Vukobratovic M, Surdilovic D, Ekalo Y, Katic D (2009) Dynamics and robust control of robot-environment interaction, vol 2. New Frontiers in Robotics, Mar 2009, World Scientific Publishing, Singapore
14. Lizama E, Surdilovic D (1996) Designing G-optimal experiments for robot dynamics identification. In: Proceedings of IEEE international conference on robotics and automation, 1996, vol 1, pp 311–316